Materials and Design 47 (2013) 566–574

Contents lists available at SciVerse ScienceDirect

Materials and Design

journal homepage: www.elsevier.com/locate/matdes

Effects of geometrical and material parameters of top and bond coats on the interfacial fracture in thermal barrier coating system

R. Xu, X.L. Fan, W.X. Zhang, Y. Song, T.J. Wang *

State Key Laboratory for Strength and Vibration of Mechanical Structures, Department of Engineering Mechanics, School of Aerospace Engineering, Xi'an Jiaotong University, Xi'an 710049, China

ARTICLE INFO

Article history:
Received 16 September 2012
Accepted 14 December 2012
Available online 2 January 2013

Keywords:
Delamination
Thermal barrier coating
Crack driving force
Finite element method

ABSTRACT

Under extreme thermal cycling delamination initiates and propagates on the interface between top coating and bond coating in thermal barrier coating (TBC) system. The objective of this work is to study the effects of geometrical and material parameters, such as the thicknesses and moduli of top and bond coats, on the interfacial delamination behavior of TBC. The interfacial crack driving force is obtained as functions of the Young's moduli of top and bond coats, the thicknesses of top coat and bond coat, etc. It is shown that in case of a stiffer top coat deposited on a relatively compliant bond coat the interfacial delamination can emerge more easily since the driving force approaches to an enormous value while emanating from the root of a channel surface crack. It is concluded that interfacial delamination can easily be initiated for a thick, stiff top coat. Considering the thermal barrier and mechanical loading carrying capabilities of coatings, optimal top coat thickness exists for the optimization design of TBC structure.

© 2012 Elsevier Ltd. All rights reserved.

1. Introduction

Thermal barrier coating (TBC) system is essential to protect gas turbine blades from high temperature, oxidation and corrosion [1–4]. The failure modes of TBC can be classified into two major categories: multiple surface cracking and interfacial delamination. Usually, multiple surface cracks occur firstly and dominate the premature failure of TBC, which are followed by interfacial delamination initiated from roots of surface cracks [5].

Considerable work was focused on the strength and safety of materials and structures, such as the damage mechanisms of materials [6–9], the failure mechanisms of film/substrate system and TBC structures [10,11]. Erdogan [12] studied the singular nature of the crack-tip stress field for bonded non-homogeneous materials under shear loading. The periodic cracking of an elastic coating bonded to a homogeneous substrate has been analyzed by Schulze and Erdogan [13]. Rizk [14] considered the surface heating to investigate the periodic surface cracking of TBC. Also, finite element method was adopted to study the surface failure of TBC, such as Huang et al. [15], Fan et al. [16,17] and Zhang et al. [18]. However, it is assumed in most of the aforementioned investigations that the film is well bonded to the substrate, which ignores the fact that interface crack may be initiated due to stress concentration. Other studies concentrated on the fracture behavior of existing interface cracks caused by residual stress, thermal cycling stress, etc., such as Cotterell and Rice [19,20], Suo and Hutchinson [21], He et al. [22]. Based on their results, the interfacial delamination is believed to be the most catastrophic failure mode of film/substrate systems or multilayer structures such as TBC.

More recently, investigations focus on the interaction of interfacial delamination and surface cracks. Zhou and Kokini [23,24] presented an analytical model to investigate the effect of preset surface crack morphology on interfacial fracture of TBC under thermal shock loading. Using the cohesive zone model, Parmigiani and Thouless [25] studied the effects of fracture toughness and cohesive strength on the deflection of surface cracks. A semi-infinite model was constructed by Mei et al. [26] to obtain the driving force of an interface crack emanating from the root of a surface crack. Fan et al. [27] investigated the effect of periodic surface cracks on the interfacial fracture of TBC. It is concluded that in some cases the durability of TBC can be enhanced due to the existence of surface cracks.

Our experimental observation on the failure of TBC, as shown in Fig. 1, presents that the thicknesses of top coat, bond coat and substrate have significant effects on the failure mode of TBC. Both periodic surface cracks and interfacial delamination appeared for a relatively thick ceramic top coat, as shown in Fig 1a. On the contrary, surface cracks without interfacial delamination dominate the failure for specimen with a relatively thin film, as shown in Fig 1b. Similar phenomena were found for specimen with different material properties of top and bond coats. However, the well-known double-layer film/substrate model cannot directly predict the behavior of multi-layer system. Moreover, despite the fact that

* Corresponding author.
E-mail address: wangtj@mail.xjtu.edu.cn (T.J. Wang).

0261-3069/$ - see front matter © 2012 Elsevier Ltd. All rights reserved.
http://dx.doi.org/10.1016/j.matdes.2012.12.053

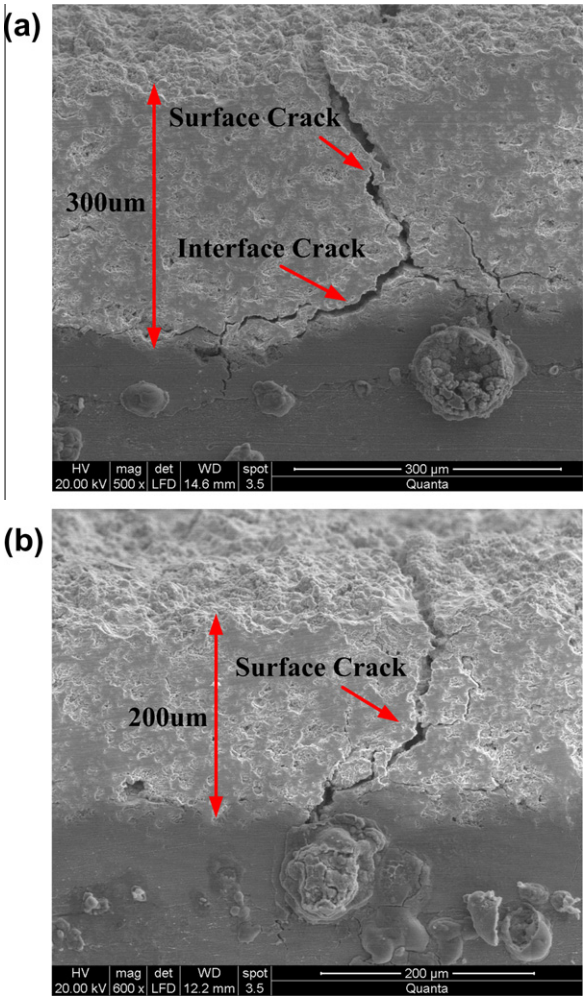

Fig. 1. Failure modes of thermal barrier coating (TBC) system: (a) a dominant surface crack with interfacial delamination and (b) surface crack without interfacial delamination.

interfacial delamination is the most important failure mode of TBC, less attention is paid directly to the variation of interfacial crack driving force for different geometrical and material parameters of each layer [23,25,26]. In addition, the previous works mostly focused on the choosing of appropriate coatings with excellent material capacity (conductivity, thermal expansivity) and microstructure to reduce the effective thermal conductivity. Whereas, less attention has been paid to how to choose appropriate coatings to ensure the mechanical capability of TBC. The objective of this work is to investigate the effects of geometrical and material parameters of components on the initiation and propagation of interfacial delamination as well as related interfacial fracture mechanisms of TBC.

2. Statement of the problem

A typical TBC structure consists of four layers, i.e. top coat (TC), bond coat (BC), a thermally grown oxide (TGO) layer between BC and TC layers, and super alloy substrate. Obviously, unavoidable mismatches of material and geometrical parameters exist between adjacent layers. As a result, the induced interface stresses can be very complex under mechanical and/or thermal loading conditions, which may lead to surface cracks or interfacial delamination. In practice, actual spalling failure of TBC begins with multiple surface cracks, and then channel surface cracks form and interfacial delaminations appear at the roots of channel cracks, as shown in Fig. 2a. Based on our experimental observations, the distance between adjacent surface cracks is generally constant (roughly twenty to thirty times TC thickness) [27]. Previous studies demonstrated that the driving force of channeling cracks in multilayer structure is independent of tunnel depth when the propagation of surface cracks reaches a steady-state [28]. Therefore, a three-dimensional (3D) TBC problem can be characterized by a two-dimensional (2D) plane strain model while investigating its fracture behavior [28]. Fig. 2b shows the simplified 2D plane strain model of steady-state multiple channel cracks accompanied with interface cracks, where h_{TC}, d and W are the TC thickness, the deflected interface crack length, and the surface crack spacing, respectively.

To consider the initiation of an interface crack from the root of a surface crack, a unit cell model can be constructed by using periodic boundary conditions [29,30], as shown in Fig. 3. The geometry mismatch between adjacent layers can be described by a non-dimensional parameter κ. Similarly, the material mismatch between adjacent layers can be represented by two non-dimensional Dundurs' parameters α and β [31]. For the plane strain problem, the parameters κ and Dundurs' parameters α, β can be expressed as

$$\kappa = \frac{h_1 - h_2}{h_1 + h_2} \tag{1}$$

$$\alpha = \frac{\bar{E}_1 - \bar{E}_2}{\bar{E}_1 + \bar{E}_2} \tag{2}$$

$$\beta = \frac{1}{2}\frac{\mu_1(1-2\nu_2) - \mu_2(1-2\nu_1)}{\mu_1(1-\nu_2) - \mu_2(1-\nu_1)} \tag{3}$$

where $\bar{E}_i = E_i/(1-\nu_i^2)$, E_i, ν_i and μ_i $(i = 1,2)$ are the plane strain modulus, Young's modulus, Poisson's ratio, and shear modulus of TBC components, respectively. For homogeneous materials, the Dundurs' parameters are written as $\alpha = \beta = 0$.

The crack flank displacement (δ_1, δ_2) and stress fields $(\sigma_{12}, \sigma_{22})$ with a distant r ahead of the kinked interface crack tip can be written as [28].

$$\delta_2 + i\delta_1 = \frac{8}{(1+2i\varepsilon)\cosh(\pi\varepsilon)}\frac{K}{E^*}\left(\frac{r}{2\pi}\right)^{1/2} r^{i\varepsilon} \tag{4}$$

$$\sigma_{22} + i\sigma_{12} = K(2\pi r)^{-1/2} r^{i\varepsilon} \tag{5}$$

where $\frac{1}{E^*} = \frac{1}{2}\left(\frac{1}{E1} + \frac{1}{E2}\right)$, $i = \sqrt{-1}$ and $r^{i\varepsilon} = \cos(\varepsilon \ln r) + i\sin(\varepsilon \ln r)$. The constant ε represents the singularity of crack tip field, which can be defined as $\varepsilon = \frac{1}{2\pi}\ln\frac{1-\beta}{1+\beta}$.

The complex stress intensity factor (SIF) K is

$$K = K_1 + iK_2 = k_1 d^{1/2-\lambda}[C(\alpha,\beta)d^{i\varepsilon} + D(\alpha,\beta)d^{-i\varepsilon}] \tag{6}$$

where K_1 and K_2 correspond to the relative normal and shear separation of crack faces, respectively, λ is a real constant and depends on Dundurs' parameters, d is the interfacial delamination length, C and D are dimensionless complex valued functions of α and β.

Stress is complex on the interface of two different materials, which leads to the mixed mode nature of the propagation of interfacial delamination. In this case, mode mixity ψ is commonly adopted to measure the relative amount of mode II and mode I at a fixed distance ahead of the crack tip, which is defined by

$$\psi = \tan^{-1}\left(\frac{\sigma_{12}}{\sigma_{22}}\bigg|_{r=l}\right) = \tan^{-1}\left(\frac{\mathrm{Im}Kl^{i\varepsilon}}{\mathrm{Re}Kl^{i\varepsilon}}\right) \tag{7}$$

where l is a reference length. To predict the mixed fracture mode of a bi-material system, an in-plane length is preferred. The TC thickness h_{TC} is chosen as the reference length herein. Noteworthily, the aforementioned formulas proposed for a two-layer structure are

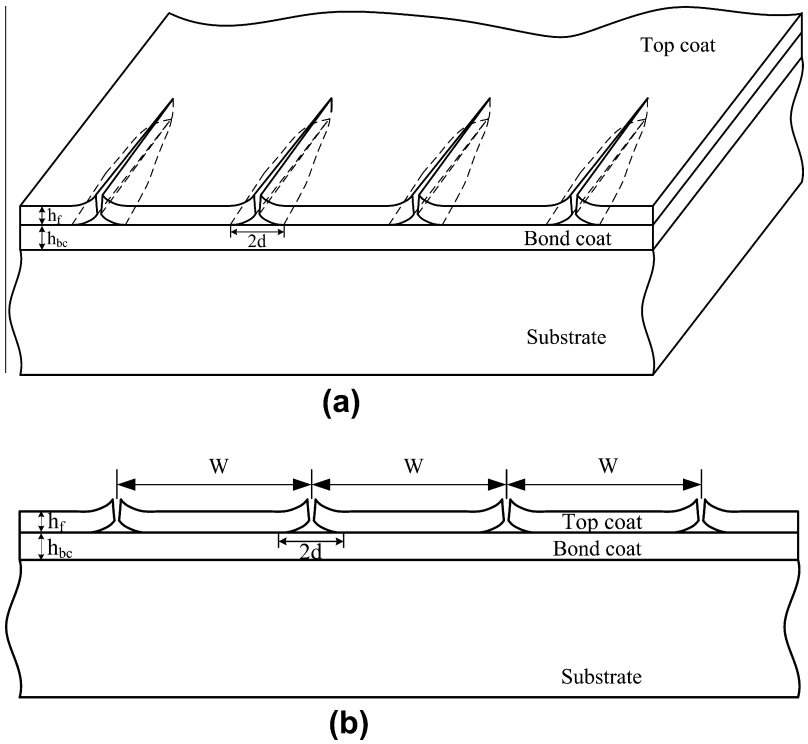

Fig. 2. The geometry of TBC with multiple surface cracks and interfacial delaminations. (a) The three dimensional configuration and (b) the corresponding two-dimensional plane strain model.

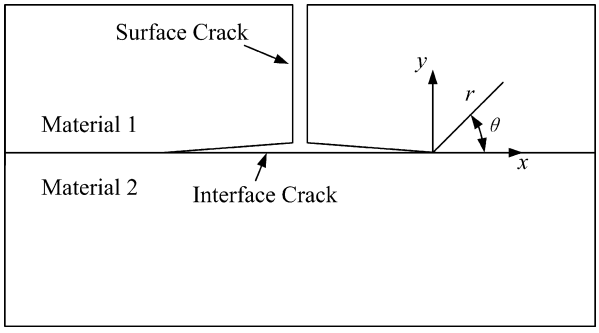

Fig. 3. Geometry and local coordinates of an interface crack initiating from the root of a surface crack.

suitable for the investigation of interfacial delamination between TC and BC layers in TBC.

Strain energy release rate (SERR) is another basic concept to study the driving force of an interface crack. A larger SERR value of the interface crack tip presents the more probability of interfacial delamination. Therefore, we can explain the interface fracture of TBC by the mean of calculating SERR. Since it is intractable to calculate K_1 and K_2 for an interface crack, the more convenient calculation of SERR is applied in this paper. The energy release associated with crack growth is characterized and calculated by *J*-integral method. On the basis of linear elastic fracture mechanics, the SIF and the SERR can be related to the value of *J*-integral. For a virtual crack advance $\lambda(s)$, the value of *J*-integral can be calculated by [32]

$$\bar{J} = \int_A \lambda(s)\mathbf{n}\cdot\mathbf{H}\cdot\mathbf{q}dA \tag{8}$$

where *dA* is the total areas of a layer of elements enclosing the crack tip, $\boldsymbol{n}$ is the outward normal vector to the corresponding integral contour, and $\boldsymbol{q}$ is the direction of virtual crack extension, $\boldsymbol{H}$ is given by

$$\mathbf{H} = \left(W\mathbf{I} - \sigma\cdot\frac{\partial\mathbf{u}}{\partial\mathbf{x}}\right) \tag{9}$$

where *W* is strain energy. For elastic material, *W* is the elastic strain energy, while for elastic–plastic or elasto-viscoplastic material, *W* is defined as the sum of elastic strain energy and plastic dissipation energy, thus represents the strain energy in an "equivalent elastic material".

Herein, the finite element code ABAQUS is employed for numerical calculations. For the plane strain tri-layer problem, as shown in Fig. 2, the corresponding boundary conditions are shown in Fig. 4a. Regarding the periodicity of the problem, nodes are allocated in pair at the left and right boundaries of the representative cell model with periodic conditions applied to keep the opposite edges deform parallel in a tangential sense [29]. A tensile load is applied to the cell model, as shown in Fig. 4a. Non-uniform mesh is adopted for the typical finite element model of the tri-layer TBC. Eight-node bilinear plane strain quadrilateral reduced integration elements are selected for all three layers except the crack tip region, where very fine mesh of singular elements are constructed, as shown in Fig. 4b. In addition, The *J*-integral values are independent to the mesh configuration if the mesh configuration is fine enough around the crack tip.

To accurately calculate the *J*-integral, fine mesh is set near the crack tip and the contour integral regions, as shown in Fig. 5. In addition, crack growth direction is assumed to be along the TC/BC interface. In ABAQUS, the first layer of elements enclosed the crack front is used to calculate the first contour integral. Since the first few contour integrals is defined by specifying the nodes close to the crack tip, the corresponding *J*-integral values may be inaccurate. To get accurate value of *J*-integral, more contours should be set, as shown in Fig. 5. The convergence of *J*-integral is

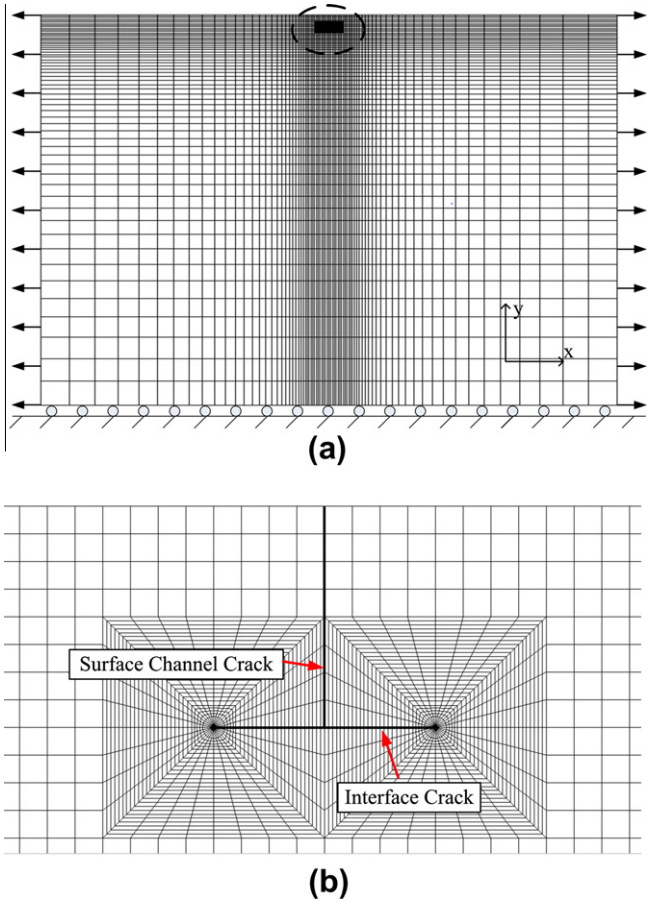

Fig. 4. (a) Finite element model of tri-layer TBC and (b) a typical mesh around the interface crack tip.

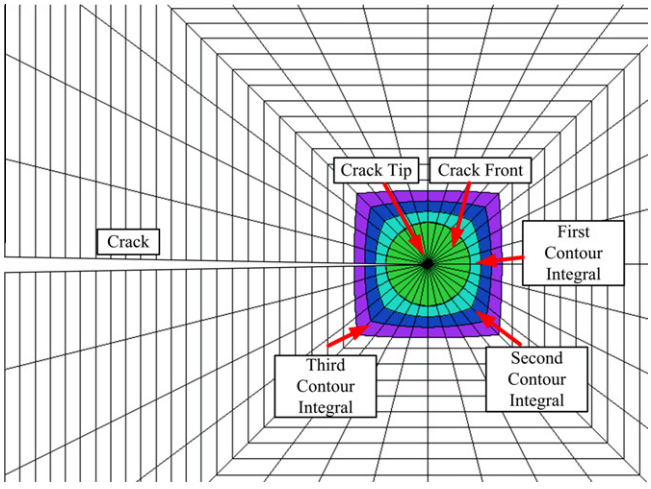

Fig. 5. Characteristic of the contour integrals around an interface crack tip.

ensured once the difference between two adjacent integral contours can be ignored.

Herein, each layer in TBC is taken to be homogeneous, isotropic and linear elastic materials. The initial geometrical and material properties are h_{TC} = 0.4 mm, h_{BC} = 0.2 mm, h_s = 30 mm, E_{TC} = 50 GPa, E_{BC} = 100 GPa, E_s = 211 GPa, $v_S = v_{BC} = v_{TC} = 0.3$ and $W/h_{TC} = 20$, where the subscripts TC, BC and S represent top coat, bond coat and substrate, respectively. In particular, wide ranges of geometrical and material parameters of each layer are analyzed to examine their effects on the driving force of interfacial delamination [33,34]. The interfacial delamination length d is considered to be in the range from zero to half of TC thickness, where the driving force (i.e. SERR) remains stable and the edge effect can be neglected.

3. Results and discussions

3.1. Effect of geometrical parameter

Mode mixity ψ and SERR G can be adopted to detailedly describe the initiation and propagation of the interfacial delamination. ψ is an important parameter to determine the fracture mode and the component ratio of driving force represented by interface SERR. As mode mixity ψ varies, the dominant fracture mode of an interface crack changes. In the case of ψ<45°, mode I fracture, which corresponds to normal separation of crack faces, dominates the interfacial fracture. In contrast, mode II plays a major role in the case of ψ>45°. In this case, crack faces usually present a shear separation. Fig. 6 shows the effect of TC thickness on the mode mixity ψ of interface crack. The variation of ψ is plotted as a function of interfacial delamination length for the case of h_{BC} = 0.2 mm E_{TC} = 50 GPa, and E_{BC} = 100 GPa. In this case, ψ is relatively small during the initiation of interfacial delamination, as shown in Fig. 6. However, ψ enhances dramatically as delamination length increases and finally reaches a stable state as the interfacial delamination length reaches about d/W = 0.025. According to the stable value of ψ shown in Fig. 6, we can conclude that mode II dominants the interfacial fracture for a sufficiently long delamination. In addition, the percentage of mode II is larger for a thinner TC (e.g. ψ is larger for h_{TC} = 0.1 mm than that of h_{TC} = 0.6 mm). Note that for a relatively thin TC case (e.g. h_{TC} = 0.1 mm) mode mixity ψ increases to its steady-state, which has been observed and defined in previous work [27,28], rapidly but oscillates. On the contrary, ψ approaches the steady value slowly and monotonically for relatively thick TC (e.g. h_{TC} = 0.6 mm). This indicates that it is easier for mode II to dominant the interfacial fracture in case of thinner TC layers.

Fig. 7 shows the mode mixity ψ as a function of interfacial delamination length for different BC thicknesses. In these cases, the following materials and geometries are selected: h_{TC} = 0.4 mm, E_{TC} = 50 GPa and E_{BC} = 100 GPa. The value of ψ rises to a stable state from a relatively small value as the interfacial delamination propagates along the interface. Obviously, the increases of ψ is more smooth than the curves shown in Fig. 6. For example, unlike the effect of TC thickness, the variation of ψ is monotonous for all BC

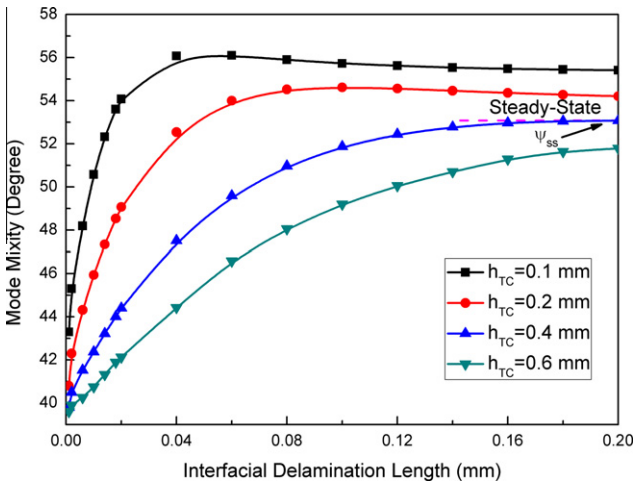

Fig. 6. Mode mixity ψ as a function of interfacial delamination length for different TC thicknesses.

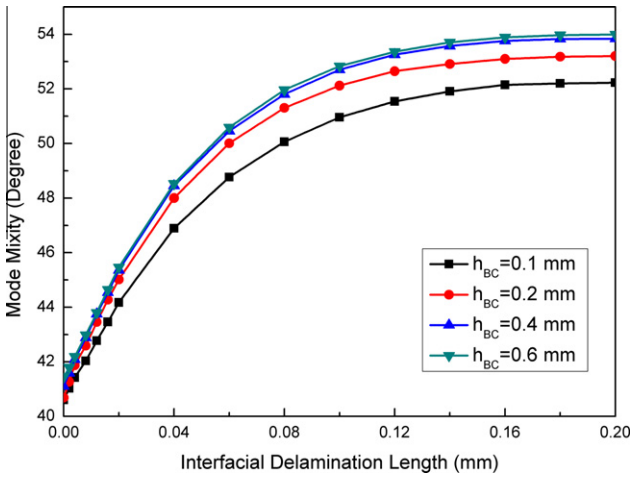

Fig. 7. The mode mixity ψ as a function of interfacial delamination length for different BC thicknesses.

thicknesses. Focused on the stable values of ψ that are larger than 45° for all the BC thicknesses considered herein, we can easily perceive that mode II dominants the interfacial delamination inevitably. Furthermore, Fig. 7 suggests that there may be an asymptotic curve for very high values of BC thickness (e.g. h_{BC} = 0.6 mm).

To obtain a clear understand about the dominant fracture mode during the stable propagating of the interfacial delamination, we compare the effects of TC and BC thickness on the steady-state mode mixity ψ_{SS}, which is essential to determine the fracture mode after the interfacial delamination reaches a sufficient length, using the unified geometry parameter κ defined by Eq. (1). Combining the steady-state mode mixity ψ_{SS} shown in Fig. 6 and Fig. 7, the relationship between ψ_{SS} and the geometry parameter κ is presented in Fig. 8. The variation of ψ_{SS} is similar for different cases, as shown in Fig. 8. For the case of setting h_{BC} as a constant and varying h_{TC}, ψ_{SS} decreases significantly with the thickening of TC(the black curve), which contributes the increases of parameter κ. The decreasing of ψ_{SS} may lead to the domination of mode I. Thus the fracture mode may transform from mode II to mode I if parameter κ increases to a critical value. However, the value of ψ_{SS} also declines as the increases of parameter κ (the red curve) caused by h_{BC} decreasing with a constant h_{TC}. Note that the declines of ψ_{SS} in this case (h_{BC} decreasing with a constant h_{TC}) is not as significant as the former case (h_{TC} increasing with a constant h_{BC}), which means that ψ_{SS} is more sensitive to TC thickness.

The effect of TC thickness on the driving force of interface crack is shown in Fig. 9, where the SERR value varies as a function of interfacial delamination length for different TC thicknesses. Instead of a monotonic variation with the delamination length, SERR oscillates in the processes of initiation and propagation of interfacial delamination. The oscillation leads to a local maximum value of SERR G_{max}, which is critical to estimate the emanation of interfacial delamination. Then, SERR declines until a steady-state is reached. Finally, beyond a certain delamination length (roughly equal to d/W = 0.05) SERR becomes almost independent of the delamination length. Herein, the corresponding G_{ss} is an important parameter to describe the driving force of stable spreading of interfacial delamination.

It is noteworthy that the oscillation of SERR cannot be eliminated by changing TC thickness. In the case of a larger h_{TC}, the appearance of G_{max} is postponed and the G_{max} is enlarged as h_{TC} increases. For a relatively thick TC the interfacial delamination will propagate to a longer distance before SERR rises to its maximum value. In addition, a thicker TC layer will induce a much higher maximum SERR which may facilitate the initiation of interfacial delamination. It should also be noted that higher stable values of SERR G_{ss} are achieved as the TC thickness h_{TC} increases. For a thicker TC, the interface crack is easier to propagate once it initiated from the root of surface cracks. This is due to the fact that a much higher stable value of SERR is achieved in this case. Considering the effect of TC thickness on the mode mixity ψ in Fig. 6, it is conclude that for thicker TC the dominant fracture mode of the easy-propagating interface crack is mode I at the initiation and gradually transfers to mode II during the propagation. The numerical results coincide with our experiment results, as shown in Fig. 1a. The same phenomenon has also been observed by Qian et al. [35] and Zhou et al. [36].

The variation of SERR as a function of interfacial delamination length is shown in Fig. 10 for different BC thicknesses. High lever stable state SERR value is achieved as h_{BC} increases. As might be intuitively expected, the SERR with the interfacial delamination only depends on the thickness of film (first layer) and is independent to the substrate (second layer) in the film/substrate systems. In this context, the results, plotted in Fig. 7, indicate that the BC (second layer) plays a non-negligible role in determining the value of SERR since there exists an extra constraint (third layer) in TBC system. Similar to the effect of TC thickness, thicker BC may

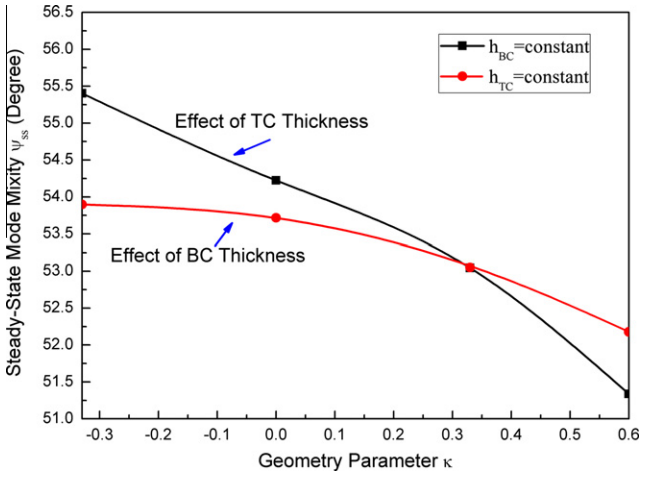

Fig. 8. The stable values of interfacial delamination mode mixity ψ_{SS} as a function of parameter κ.

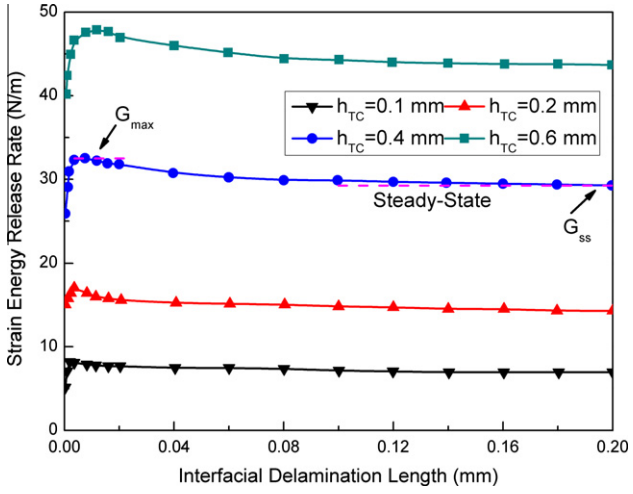

Fig. 9. The strain energy release rate as a function of interfacial delamination length for different TC thicknesses. The G_{max} stands for the maximum value of strain energy release rate.

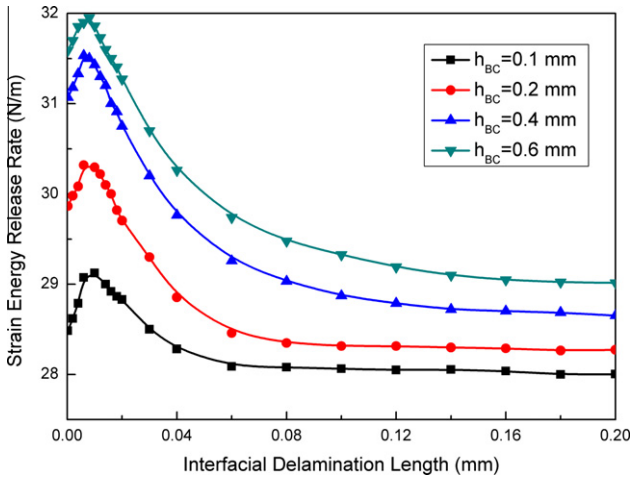

Fig. 10. The strain energy release rate as a function of interfacial delamination length for different BC thicknesses.

obviously result in the increases of the maximum SERR (e.g. h_{BC} = 0.6 mm). But comparing with the enlargement of SERR caused by TC geometry, the increases of SERR due to the thickening of BC is much smaller. Combining the results shown in Figs. 9 and 10, we can conclude that both the stable and maximum SERR values rise with the thickening of TC and/or BC. The difference is that the TC thickness is a more significant factor that affects the evolution of SERR. The detail comparison of the effects of TC thickness and TC thickness on SERR will be obtained from Fig. 11.

The effects of TC and BC geometries on the driving force of delamination are shown in Figs 9 and 10, respectively, in which the obvious increase of SERR corresponding to thickening TC and/or BC can be noted. The effects of TC and BC thicknesses on the stable driving force of interfacial delamination are shown in Fig. 11, in which the stable value of SERR G_{ss} is functions of the geometry parameter κ. It is seen that the stable SERR rises with enlarging the geometry parameter κ, which may be caused by the thickening of TC or thinning BC as the definition by Eq. (2). Noteworthily, the stable SERR rises dramatically in the case of setting h_{BC} as a constant and varying h_{TC} (the black line in Fig. 11) , which means that the SERR is only affected by h_{TC}. On the contrary, the variation of SERR for setting h_{TC} as a constant and varying h_{BC} (the red line in Fig. 11) can be almost negligible compared to the former. Obviously, it can be concluded that the driving force of stable propagation of interfacial delamination is mainly determined by h_{TC} rather than h_{BC}.

3.2. Effect of material parameter

Ye et al. [37] investigated the effect of material mismatch parameter α on the driving force of interfacial delamination. They concluded that for film/substrate systems of stiffer films deposited on relatively compliant substrate ($\alpha > 0$), the interfacial delamination could more likely to occur than relatively compliant films on stiffer substrate ($\alpha < 0$). Herein, we consider the effect of material parameter of each layer (especially TC and BC) on the delamination driving force. After obtaining the effect of material on the driving force, we can explain the reason why TBC with stiff TC and soft BC is more likely to fracture on the interface, which is found in our test. In this section, the effects of material parameters E_{TC} and E_{BC}, which determines the value of α defined by Eq. (2), are discussed in details.

Fig. 12 shows the variation of ψ as a function of interfacial delamination length for different Young's moduli of TC. The geometries constants and materials of TC and BC except E_{TC} are fixed as followings, h_{TC} = 0.4 mm, h_{BC} = 0.2 mm and E_{BC} = 100 GPa. As Fig. 12 shown, ψ rises dramatically at the beginning of the interfacial delamination and then approaches to a relatively stable state as the crack propagates along the interface. For the stiffer TC (e.g. $E_{TC.}$ = 150 GPa and E_{TC} = 200 GPa), ψ rises more rapidly with the propagation of the delamination than that for more compliant TC (e.g. E_{TC} = 50 GPa), which implies that the domination of mode II fracture comes much earlier. However, it should be noted that for the case that the moduli of TC is smaller than that of BC (mismatch parameter $\alpha < 0$, e.g. E_{TC} = 50 GPa), the steady value of ψ stays negligibly higher (ψ_{ss}52°) when compared with the case α = 0 (e.g. E_{TC} = 100 GPa) or $\alpha > 0$ (e.g. E_{TC} = 150 GPa and E_{TC} = 200 - GPa), which both asymptotically approach to a same steady-state value (ψ_{ss} = 51°). It is of interest that this is very close to the results of Mei et al. [26], which present a value of 52° for the film/substrate model that the film and the substrate have identical elastic moduli.

The relationship between mode mixity ψ and interfacial delamination length for different Young's moduli of BC is shown in Fig. 13. Fixed the material and geometry of TC and BC except E_{BC} as followings, h_{TC} = 0.4 mm, h_{BC} = 0.2 mm and E_{TC} = 100 GPa. Comparing with Fig. 13, we can obtain similar results that ψ rises

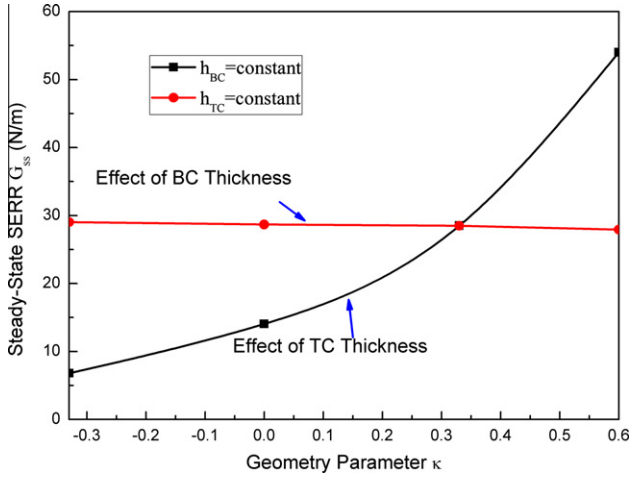

Fig. 11. The stable values of interfacial delamination SERR G_{SS} as a function of aggregate thicknesses of BC and TC.

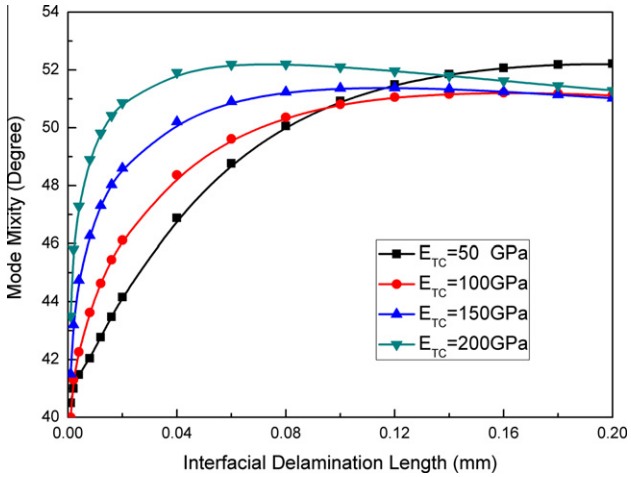

Fig. 12. The mode mixity ψ as a function of interfacial delamination length for various Young's moduli of TC.

rapidly for compliant BC (e.g. E_{BC} = 50 GPa) while ψ rises slowly and monotonically for stiff BC (e.g. E_{BC} = 200 GPa). It should be noted that E_{BC} has a significant effect on the steady-state value of ψ. Obviously, the steady-state value ψ_{SS} emerges as the E_{BC} increases, which means that during the propagation of the interfacial delamination the percentage of mode II is quite larger for the systems with a stiffer BC.

Combining the steady-state mode mixity ψ_{SS} shown in Fig. 12 and Fig. 13, the relationship between ψ_{SS} and material mismatch parameter α is presented in Fig. 14. It is well know that both Young's moduli of TC (E_{TC}) and BC (E_{BC}) make contribution to the material mismatch parameter α. While setting E_{TC} to a constant, the variation of α is caused by E_{BC} solely, likewise, E_{TC} is the only impact factor to α if E_{BC} keeps a constant. In this way, the effects of material properties of TC and BC on the steady-state mode mixity of delamination can be combined and compared through the unified parameter α. In Fig. 14, ψ_{SS} always drops with the increases of α, which may be caused by either hardening TC or softening BC. Consequently, the percent of mode II fracture reduces during the propagation of interfacial delamination. Obviously, more attention should be paid on the mode I fracture during delamination if the TBC is deposited with an enhanced material mismatch parameter α. Note that the ψ_{SS} reduces more rapidly while softening the BC, which means that the Young's moduli of BC has a more notable effect on ψ_{SS}. Therefore, the deposition of the BC also needs a special attention.

Fig. 15 shows the SERR as a function of interfacial delamination length for various E_{TC}. It is seen from Fig. 15 that Young's modulus of TC layer has significant effect on the driving force of interfacial delamination. The value of SERR rises with the increase of normalized Young's modulus E_{TC}. Comparing with relatively compliant TC (e.g. E_{TC} = 50 GPa), the stable value of SERR for stiffer TC (E_{TC} = 100 - GPa) is much larger (roughly five times that of E_{TC} = 50 GPa). Moreover, in the case of a compliant TC (e.g. E_{TC} = 50 GPa), SERR oscillates in the process of interfacial delamination emanation, which coincides with the results obtained by Ye et al. [37] and Mei et al. [26]. The non-dimensional SERR of the interface crack in film/substrate system calculated by Ye et al. [37] and Mei et al. [26] becomes unbounded as interfacial delamination length approach to zero for systems having films stiffer than substrates. However, for more compliant films, the maximum SERR exists.

However, due to the remarkable influence of Young's modulus of TC, the oscillation of SERR can be ignored while examining the evolution of SERR for different elastic material mismatches (e.g. E_{TC} = 150 GPa). As a result, for relatively compliant TC it seems that the SERR varies monotonically with the increase of interfacial delamination length until a relative steady-state is reached, as shown in Fig. 15. On the contrary, for a relatively stiff TC the SERR is closely related to the delamination length especially during the initiation of interfacial delamination. In details, the SERR approaches an enormous value as delamination length approaches to zero, which may easily result in interfacial delaminations.

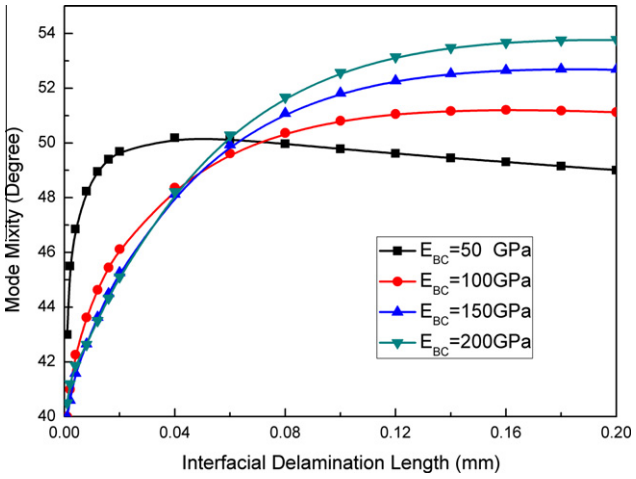

Fig. 13. The mode mixity ψ as a function of interfacial delamination length for different Young's moduli of BC.

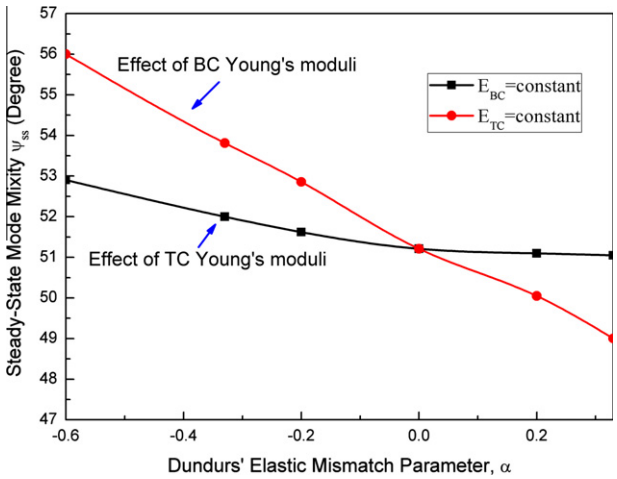

Fig. 14. The stable values of interfacial delamination mode mixity ψ_{SS} as a function of material mismatch parameter α.

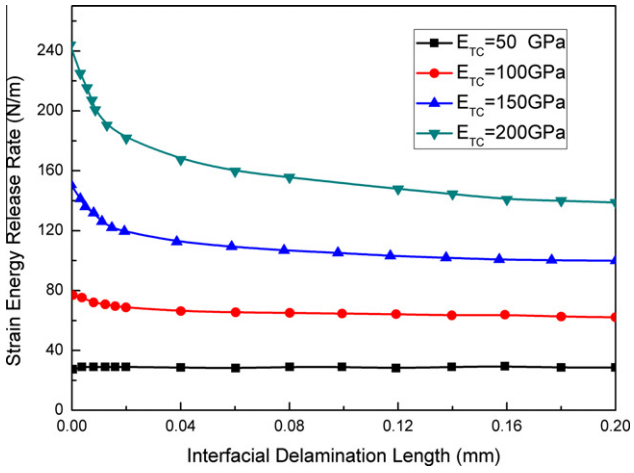

Fig. 15. The strain energy release rate as a function of interfacial delamination length for various Young's moduli of TC.

The effect of E_{BC} on the driving force of interfacial delamination is shown in Fig. 16. For relatively compliant TC deposited on stiffer BC (e.g. E_{BC} = 200 GPa), the interfacial delamination driving force approximately approaches to zero as delamination length approaches to zero, which implies that in this case the driving force will vanish at the root of the surface channel crack. On the contrary, in the case of compliant BC (e.g. E_{BC} = 50 GPa), the SERR becomes unbounded as delamination length approaches to zero, which means the interfacial delamination is much easier to initiate. Obviously, the SERR drops with increasing Young's modulus of BC, which is insignificant, however, for relatively stiff BC (e.g. E_{BC} > 50 GPa). As a result, in some cases (e.g. E_{BC} = 200 GPa), the local maximum SERR is even larger than the stable value for those with relatively compliant BC (e.g. E_{BC} = 100 GPa). In general, the stable SERR value declines monotonically as Young's modulus of BC increases.

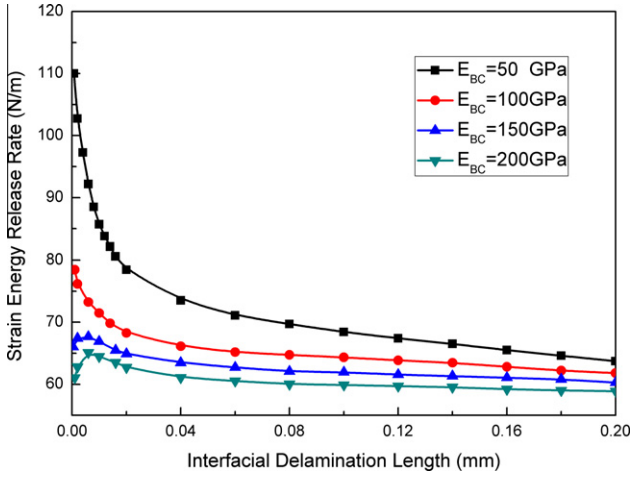

Fig. 16. The strain energy release rate as a function of interfacial delamination length for various Young's moduli of BC.

The effects of material properties of TC and BC on the driving force of delamination are investigated and shown in Figs 15 and 16, respectively. The effects of material properties of TC and BC on the stable driving force (G_{SS}) of delamination can be combined and compared through the unified parameter α, as shown in Fig. 17, where the stable value of the interfacial delamination SERR are plotted as functions of material mismatch parameter α. when E_{BC} equals to a constant, the variation of G_{SS} is affected by changing E_{TC}, which is corresponding to Fig. 15. Similarly, the red curve presents the relationship between G_{SS} and E_{BC} while E_{TC} is constant. The stable SERR rises as the elastic material mismatch parameter α increases, i.e. the Young's modulus of TC increases or the Young's modulus of BC decreases. However, as α increases, the stable SERR value is more remarkably affected for a given constant BC modulus E_{BC} compared to that of given constant TC modulus E_{TC}. For example, changing the E_{TC} to make parameter α rises from −0.6 to 0.33 can lead to the steady-state SERR increasing from 13.6 N/m to 132.6 N/m (increase 875%), while the steady-state SERR increases from 56.2 N/m to 61.2 N/m (increase only 8.9%) when change E_{BC}. Therefore, it is clear that the propagation of interfacial delamination can be postponed or suppressed easily by softening TC instead of hardening BC. Combined the results of Fig. 14 and Fig. 17, it is concluded that the steady-state mode mixity ψ_{SS} is mainly affected by the Young's modulus of BC and in contrast the steady-state SERR G_{SS} seems to be determined by the Young's modulus of TC.

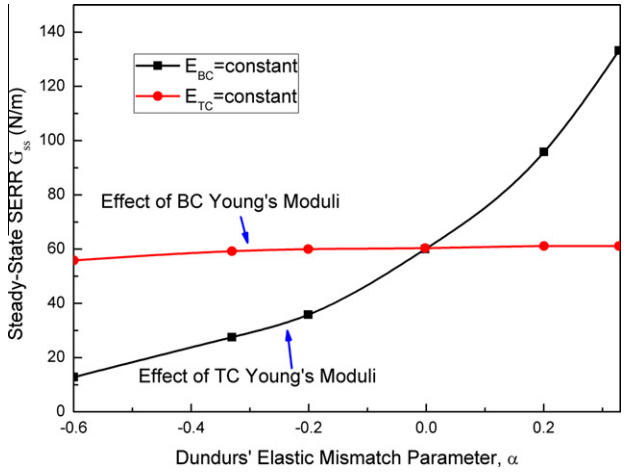

Fig. 17. The stable values of interfacial delamination SERR G_{SS} as a function of material mismatch parameter α.

4. Conclusions

The effects of geometrical and material parameters of top and bond coats on the failure mechanisms of thermal barrier coating system (TBC) were investigated in this work. The results show that the delamination driving forces are more sensitive to the thickness of ceramic top coat than that of bond coat. In addition, interfacial delamination can easily initiate and propagate for relatively thick top coat since the strain energy release rate increases drastically with the thickening of top coat. Therefore, to suppress or postpone the interfacial failure of TBC, relatively thin top coat layer and good interfacial shear strength are recommended for the structure design of TBC. The effects of material parameters of top and bond coats on the interfacial delamination are also significant. In the case of a stiffer top coat deposited on a relatively compliant bond coat, the interfacial delamination can extend more easily since the interfacial delamination driving force approaches to an enormous value while emanating from the root of a channel surface crack. It is also seen that softening the top coat or hardening the bond coat can make a contribution to slow down the propagation of delamination. Moreover it is much easier to postpone or suppress the initiation and propagation of interfacial delamination by softening the top coat than hardening the bond coat because the driving force of delamination is more sensitive to the Young's modulus of top coat. Considering the thermal barrier and mechanical loading carrying capabilities simultaneously, optimal design of the thicknesses of top coat and bond coat are preferable for TBC structure. Further study is aimed to perform the optimal design of top coat thickness for given performance requirements.

Acknowledgements

This work is supported by the State 973 Program of China (2013CB035701), NSFC (11272259, 11021202,11002104 and 11172227), and MOE fund.

References

[1] Miller RA. Current status of thermal barrier coatings–An overview*1. Surf Coat Technol 1987;30:1–11.
[2] Evans AG, Mumm D, Hutchinson J, Meier G, Pettit F. Mechanisms controlling the durability of thermal barrier coatings. Prog Mater Sci 2001;46:505–53.
[3] Padture NP, Gell M, Jordan EH. Thermal barrier coatings for gas-turbine engine applications. Science 2002;296:280.
[4] Wang L, Wang Y, Sun XG, He JQ, Pan ZY, Wang CH. A novel structure design towards extremely low thermal conductivity for thermal barrier coatings – Experimental and mathematical study. Mater Des 2012;35:505–17.
[5] Yang L, Zhou Y, Mao W, Lu C. Real-time acoustic emission testing based on wavelet transform for the failure process of thermal barrier coatings. Appl Phys Lett 2008;93:231906.
[6] Wang TJ, Lou Z. A continuum damage model for weld heat affected zone under low cycle fatigue loading. Eng Fract Mech 1990;37:825–9.
[7] Wang TJ. Further investigation of a new continuum damage mechanics criterion for ductile fracture: experimental verification and applications. Eng Fract Mech 1994;48:217–30.
[8] Bai Y, Han Z, Li H, Xu C, Xu Y, Wang Z, et al. High performance nanostructured ZrO2 based thermal barrier coatings deposited by high efficiency supersonic plasma spraying. Appl Surf Sci 2011.
[9] Ranjbar-far M, Absi J, Mariaux G, Smith DS. Crack propagation modeling on the interfaces of thermal barrier coating system with different thickness of the oxide layer and different interface morphologies. Mater Des 2011;32:4961–9.
[10] Hu M, Evans AG. The cracking and decohesion of thin films on ductile substrates. Acta Metall 1989;37:917–25.
[11] Lu TQ, Zhang WX, Wang TJ. The surface effect on the strain energy release rate of buckling delamination in thin film-substrate systems. Int J Eng Sci 2011.
[12] Erdogan F. The crack problem for bonded nonhomogeneous materials under antiplane shear loading. J Appl Mech 1985;52:823.
[13] Schulze GW, Erdogan F. Periodic cracking of elastic coatings. Int J Solids Struct 1998;35:3615–34.

[14] Rizk AEFA. Periodic array of cracks in a strip subjected to surface heating. Int J Solid Struct 2004;41:4685–96.
[15] Huang R, Prevost J, Huang Z, Suo Z. Channel-cracking of thin films with the extended finite element method. Eng Fract Mech 2003;70:2513–26.
[16] Fan XL, Zhang WX, Wang TJ, Liu G, Zhang J. Investigation on periodic cracking of elastic film/substrate system by the extended finite element method. Appl Surf Sci 2011;257:6718–24.
[17] Fan XL, Zhang WX, Wang TJ, Sun Q. The effect of thermally grown oxide on multiple surface cracking in air plasma sprayed thermal barrier coating system. Surf Coat Technol 2012.
[18] Zhang WX, Fan XL, Wang TJ. The surface cracking behavior in air plasma sprayed thermal barrier coating system incorporating interface roughness effect. Appl Surf Sci 2011.
[19] Cotterell B, Rice JR. Slightly curved or kinked cracks. Int J Fract 1980;16:155–69.
[20] Rice JR. Elastic fracture mechanics concepts for interfacial cracks. J Appl Mech Trans ASME 1988;55:98–103.
[21] Suo Z, Hutchinson JW. Interface crack between two elastic layers. Int J Fract 1990;43:1–18.
[22] He MY, Evans AG, Hutchinson JW. Crack deflection at an interface between dissimilar elastic materials: role of residual stresses. Int J Solids Struct 1994;31:3443–56.
[23] Zhou B, Kokini K. Effect of pre-existing surface crack morphology on the interfacial thermal fracture of thermal barrier coatings: a numerical study. Mater Sci Eng A 2003;348:271–9.
[24] Zhou B, Kokini K. Effect of surface pre-crack morphology on the fracture of thermal barrier coatings under thermal shock. Acta Mater 2004;52:4189–97.
[25] Parmigiani J, Thouless M. The roles of toughness and cohesive strength on crack deflection at interfaces. J Mech Phys Solids 2006;54:266–87.
[26] Mei H, Pang Y, Huang R. Influence of interfacial delamination on channel cracking of elastic thin films. Int J Fract 2007;148:331–42.
[27] Fan XL, Xu R, Zhang WX, Wang TJ. Effect of periodic surface cracks on the interfacial fracture of thermal barrier coating system. Appl Surf Sci 2012;258:9816–23.
[28] Hutchinson JW, Suo Z. Mixed mode cracking in layered materials. Adv Appl Mech 1992;29:191.
[29] Zhang WX, Wang TJ, Li L. Numerical analysis of the transverse strengthening behavior of fiber-reinforced metal matrix composites. Comput Mater Sci 2007;39:684–96.
[30] Xu ZM, Zhang WX, Wang TJ. Deformation of closed-cell foams incorporating the effect of inner gas pressure. Int J Appl Mech 2010;2:489–513.
[31] Dugdale D. Yielding of steel sheets containing slits. J Mech Phys Solids 1960;8:100–4.
[32] ABAQUS User's Manual. Dassault Systèmes Simulia Corporation. 2009.
[33] Evans AG, Clarke D, Levi C. The influence of oxides on the performance of advanced gas turbines. J Eur Ceram Soc 2008;28:1405–19.
[34] Wang L, Wang Y, Sun XG, He JQ, Pan ZY, Zhou Y, et al. Influence of pores on the thermal insulation behavior of thermal barrier coatings prepared by atmospheric plasma spray. Mater Des 2011;32:36–47.
[35] Qian G, Nakamura T, Berndt CC, Leigh SH. Tensile toughness test and high temperature fracture analysis of thermal barrier coatings. Acta Mater 1997;45:1767–84.
[36] Zhou YC, Tonomori T, Yoshida A, Liu L, Bignall G, Hashida T. Fracture characteristics of thermal barrier coatings after tensile and bending tests. Surf Coat Technol 2002;157:118–27.
[37] Ye T, Suo Z, Evans A. Thin film cracking and the roles of substrate and interface. Int J Solids Struct 1992;29:2639–48.